Accepted for Vehicle System Dynamics

Modeling Generalization and Property Analysis of Flexible-Wheel Suspension Concept for Planetary Surface Vehicles

Dongpu Cao[1*], Amir Khajepour[1] and Xubin Song[2]

[1]Waterloo Center for Automotive Research (WatCAR), University of Waterloo, ON, Canada
[2]Advanced Control & Automation, Eaton Corporation, MI, USA

E_mails: dongpu@uwaterloo.ca; akhajepour@uwaterloo.ca; xubinsong@eaton.com
*Corresponding author

Abstract: Planetary surface vehicles (PSVs) play a critical role in space explorations. Flexible-wheel (FW) suspension concept has been regarded to be one of the novel technologies for future PSVs, where a few experimental studies have demonstrated its potential benefits in improving tractive performance of PSVs. This study develops generalized models for fundamental stiffness and damping properties and power consumption characteristics of the FW suspension with and without considering practical wheel-hub dimensions. Compliance rolling resistance (CRR) coefficient is further defined and derived for the FW suspension. Based on the generalized models and two dimensionless property measures, suspension properties are analyzed for a few selected FW suspension configurations. The sensitivity analysis is further performed to investigate the effects of the design parameters and operating conditions on the CRR and power consumption characteristic of the FW suspension. The modeling generalization permits analyses of fundamental properties and power consumption characteristics of different FW suspension systems in a uniform and very convenient manner, which would also serve as a theoretical foundation for the design of FW suspensions for future PSVs.

Keywords: planetary surface vehicles (PSVs); flexible-wheel (FW) suspension; modeling generalization; stiffness/damping properties; compliance rolling resistance (CRR); power consumption

Nomenclature:

Parameter	Description
CRR	Compliance rolling resistance of FW suspension
C_n	Damping coefficient of unit #n
D_n	Displacement of unit #n
f	Vertical-mode natural frequency of a PSV with FW suspension
k_L, c_L	Effective rotational stiffness and damping of FW suspension in a magnitude of L, respectively
k_{Ln}, c_{Ln}	Effective rotational stiffness and damping of unit #n in a magnitude of L, respectively
k_V, c_V	Effective vertical stiffness and damping of FW suspension, respectively
k_{Vn}, c_{Vn}	Effective vertical stiffness and damping of unit #n, respectively
k_X, c_X	Effective longitudinal stiffness and damping of FW suspension, respectively
k_{Xn}, c_{Xn}	Effective longitudinal stiffness and damping of unit #n, respectively
k_α, c_α	Effective translational stiffness and damping of FW suspension in an angle of α, respectively
$k_{\alpha n}$, $c_{\alpha n}$	Effective translational stiffness and damping of unit #n in an angle of α, respectively
K_n	Stiffness of unit #n
L_0	Static vertical deflection
P_n	Power consumption of unit #n
P_S	Power consumption of FW suspension
R	Radius of the FW suspension
RPF	Rotational property factor of FW suspension
TPF	Translational property factor of FW suspension
V	Rover forward speed
V_n	Velocity of unit #n
ξ	Vertical-mode damping ratio of a rover with FW suspension
$\omega = V/(R - L_0)$	Angular velocity of OB

1. Introduction

Planetary surface vehicles (PSVs), or planetary rovers, have been demonstrated as very effective tools for space explorations on Mars and on the moon, and will continue to play their important roles in future exploration missions [1-3]. The trend for autonomous robotic explorations in the coming decades will be to explore more difficult terrains, e.g. Mars' Valles Marineris and the moon's South Pole Aitken Basin, where science data are expected to be the richest. Such operations, however, encounter many challenges including: large-scale terrain, limited resources, and dynamic occlusion of sunlight and communication that need to be studied and resolved [4]. These will necessitate long lasting PSVs capable of traversing and exploring valleys, canyons and polar regions to search for water/ice and signs of life with minimal power consumption. The human exploration missions, such as ambitious establishment of pressurized lunar habitats, would pose additional challenges on future PSV designs, such as crew transport [2,5].

Power/energy management of PSVs is a primary concern, as observed from the Mars Pathfinder and Mars Exploration Rover (MER) missions [1]. The previously proposed path planning and scheduling strategies, which have been successful in satisfying the constraints posed by the resource, are incapable of optimizing the resource usage [1]. This calls for a more effective optimization technique for the power management optimization of PSVs, which however requires a comprehensive understanding of power/energy consumption characteristics of PSVs when operating in a complex environment. This would further necessitate an enhanced understanding of fundamental properties and dynamics of PSV systems as well as their interactions with operating environments, such as terrain conditions [6].

Future PSVs should have the attributes of high mobility, reliability and stability, light weight and low energy consumption, for which a six-wheeled configuration is considered to be desirable [7-9]. Efforts have been made to develop novel PSV concepts, particularly those ideal for all-terrain performance [2,3,7-12]. These studies further emphasized the importance of PSV chassis/suspension design. However, many of the current PSV suspension design concepts could not provide a complete equalization of the wheel loads when operating on rough terrains, which directly leads to the reduced efficiency of the rover mobility system [7]. This consequently caused the previous Mars rovers to traverse distance much less than their expected daily travel, which thus necessitates a systematic investigation of the mobility and suspension systems for future PSVs [10,11]. It has also been noted that the current rover locomotion/suspension design is primarily based on knowledge of precedent robotic and traditional ground vehicles, intuition and experience, which however seldom involves systematic analysis as well as quantitative rationalization [11].

Design of conventional ground vehicle suspension and tire-wheel system involves a complex challenge, which has to be compromised among different performance measures related to ride, handling, road-holding, design space, road-friendliness, and fuel economy [13-18]. Good vehicle handling and fuel economy generally necessitate a relatively high inflation pressure in pneumatic tires, which however tends to deteriorate ride performance and road-friendliness. This is due to the strong coupling between the cornering and vertical stiffness properties of a pneumatic tire, both of which are strongly influenced by the inflation pressure. Suspension has thus been popularly employed to provide an effective isolation primarily of vertical vibrations and shocks transmitted through tire from road irregularities. This, however, would require additional design space and also tend to increase the height of vehicle center of gravity (c.g.) and design/tuning complexity, which in turn pose more challenges on chassis design and development. Pneumatic tires, when applying to conventional ground vehicles, impose safety issues due to tire deflection failure, as well as environmental issues. Apart from these, the presence of outgassing, UV and atomic oxygen degration and considerable variations in planetary

surface temperature also makes pneumatic tires and elastomers impractical in the lunar and Mars surface exploration missions [2].

Concept of flexible-wheel (FW) suspension has been recently proposed and/or investigated for future ground mobility vehicles and PSVs [2,3,12,19-24]. One of the well-known FW design examples is the Michelin Tweel, an integrated airless tire/wheel unit, which replaces the traditional tire, wheel, valve and tire-pressure monitoring system for conventional vehicle applications [23]. The FW concept generally integrates stiffness/damping components within a non-pneumatic tire and wheel system, to realize decoupled ride and handling, compact and light-weight design, enhanced traction, road-holding, road-friendliness, driving safety and fuel economy, when applied to ground mobility vehicles. It also has a potential to replace conventional vehicle suspension system.

The integration of damping components in an FW design would realize a direct and improved control over dynamic tire forces, and thus enhanced road-holding quality and vehicle traction performance, unlike conventional suspension systems that indirectly control the dynamic tire forces. The integrated damping would also help inhibit and dissipate the vehicle oscillations, particularly when operating on rough roads/terrains or passing bumps/potholes. Harrison et. al [5] noted that rovers tend to lost contact with the moon surface that leads to a momentary loss of control when encountering moderate bumps at a speed of about 13 km/h, due to the much lower gravity on the moon surface compared to that on Earth. Therefore, the inclusion of sufficient suspension damping would be particularly important for a PSV when operating on the moon and on Mars that are characterized by a much lower gravity compared to Earth [25].

The compliance in the FW suspension concept for PSVs can be realized by either metallic or composite materials, while the damping may be further realized by using high damping composite materials or other techniques [2,21,26]. A few studies have investigated FW concept applying to PSVs, and demonstrated its potential benefits on improving tractive performance mainly through experimental efforts [2,12,19]. However, there are a few fundamental issues requiring extensive studies for practical FW design and implementation for future PSVs, including:

- How to select FW design parameters to achieve desirable translational stiffness property corresponding to different FW design configurations for enhanced vibration- and shock-isolation performance for protection of on-board instrumentations and/or ride comfort of crew?
- Since in-wheel motor provides tractive force, it induces a torque applied on the FW suspension and tends to deflect the wheel in the rotation direction, which is undesirable for rover motion and traction control. Thus, it would be important to characterize the torsional stiffness property of FW designs.
- How to select FW design parameters to achieve desirable damping property corresponding to different FW design configurations for enhanced vibration- and shock-isolation performance?
- A static vehicle load will induce a static deflection on FW suspension. During driving, such static deflection combined with FW suspension damping would generate compliance rolling resistance (CRR), and therefore require certain amount of power to overcome the CRR. Thus, it would be important to understand such phenomenon and seek solutions on how to minimize the CRR and power consumption through FW design.
- Different planets exhibit different gravity characteristics. How does the gravity affect the CRR and power consumption characteristics of FW suspension?

This study develops a generalized model for stiffness/damping properties and power consumption characteristics of the FW concept. The mathematical formulations for the CRR characteristics of FW suspension are then derived from the generalized model. Sensitivity analyses are conducted to investigate the effects of different FW suspension design parameters, rover speed, and gravity on the CRR characteristics of the FW suspension.

2. Modeling Generalization of FW Suspension without Considering Wheel-Hub Dimensions

Figure 1 presents the concept of FW suspension design, where a number of stiffness-damping units are assumed to be ideally perpendicular to the wheel rim and evenly distributed when the external loads are not applied to the FW suspension. The other ends of the units are assumed to be connected to the center of the wheel, by neglecting the wheel-hub dimensions. The effect of wheel-hub dimensions will be considered and modeled in the next section. The deflections of different stiffness-damping units of the FW suspension are illustrated in Fig. 1, subject to a static vertical load and a constant rover forward speed V. L_0 represents the static vertical deflection of the FW suspension under a static vertical load.

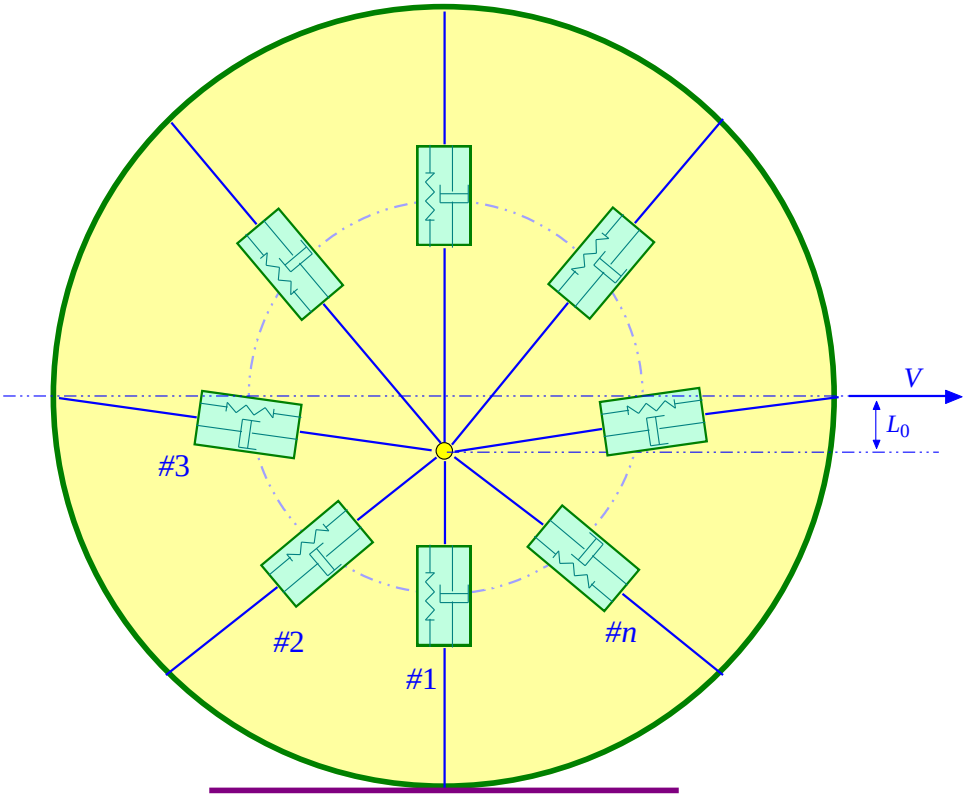

Fig. 1: Representation of the FW suspension deflections under a static vertical load and a constant forward speed (without considering wheel-hub dimensions).

2.1 MODELING OF POWER CONSUMPTION CHARACTERISTICS

In order to derive a generalized model for the FW suspension concept, an equivalent model of motion of a single spring-damper unit in the FW suspension is used, as shown in Fig. 2. The displacement D_n, velocity V_n and power consumption P_n of the spring-damper unit #n based on Figs. 1 and 2, such that:

$$D_n = \sqrt{R^2 + L_0^2 - 2RL_0\cos(\omega t + 2\pi(n-1)/n)}$$

$$V_n = \frac{dD_n}{dt} = \frac{RL_0\omega\sin(\omega t + 2\pi(n-1)/n)}{\sqrt{R^2 + L_0^2 - 2RL_0\cos(\omega t + 2\pi(n-1)/n)}}$$

$$P_n = C_n V_n^2 = C_n \frac{R^2 L_0^2 \omega^2 \sin^2(\omega t + 2\pi(n-1)/n)}{R^2 + L_0^2 - 2RL_0\cos(\omega t + 2\pi(n-1)/n)} \tag{1}$$

where R is the radius of the FW suspension, and $\omega = V/(R - L_0)$, which is the angular velocity of OB, and C_n is the damping coefficient of unit #n.

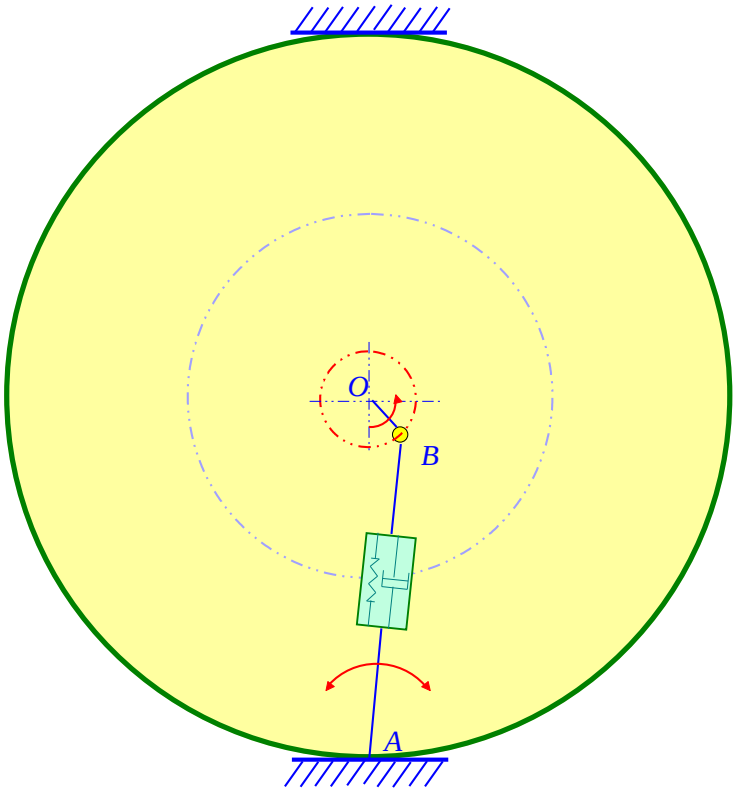

Fig. 2: Modeling simplification of the FW suspension (without considering wheel-hub dimensions).

The overall power consumption P_S of the FW suspension can be derived from Eq. (1), such that:

$$P_S = P_1 + P_2 + \cdots + P_n = \sum_{j=1}^{n} \frac{C_j R^2 L_0^2 \omega^2 \sin^2(\omega t + 2\pi(j-1)/n)}{R^2 + L_0^2 - 2RL_0\cos(\omega t + 2\pi(j-1)/n)} \tag{2}$$

It can be observed from Eqs. (1) and (2) that the power consumption characteristics of different spring-damper units in an FW suspension only differ by a time delay or lead. This indicates that for a considerably long time driving, the energy consumption due to each unit can be considered to be identical if the stiffness and damping properties of each unit are identical, which suggests an identical power consumption characteristic for each spring-damper unit.

Assuming the damping coefficients of different spring-damper units are constant and equal to *C*, the average power consumption $P_{S_{AVE}}$ can be derived from Eq. (2) for a long time-period, such that:

$$P_{S_{AVE}} = \frac{nCR^2L_0^2\omega}{T}\int_0^{\omega T}\frac{\sin^2(q)}{R^2+L_0^2-2RL_0\cos(q)}d(q) \tag{3}$$

The above formulation indicates that the power consumption of the FW suspension is directly related to the radius of the suspension wheel, the number of spring-damper units, the damping coefficient of each unit, the static vertical deflection of suspension as well as the vehicle forward speed. However, the FW suspension wheel radius is dependent upon the requirement of PSV design and packaging, while the static vertical deflection is a function of vertical wheel load and effective vertical stiffness of the FW suspension. The effective vertical stiffness of the FW suspension is determined by the number of spring-damper units involved and stiffness property of each unit, while damping coefficient of each unit is related to the effective vertical damping of the FW suspension and the number of spring-damper units. In order to analyze the power consumption characteristic of the FW suspension concept and to obtain the fundamental relationships between power consumption of the FW suspension and various system design and operating parameters, it is necessary to identify the effective stiffness and damping properties of the FW suspension.

2.2 MODELING OF STIFFNESS AND DAMPING PROPERTIES

The effective stiffness and damping properties (e.g. in vertical or longitudinal direction) are strongly related to the number of spring-damper units and stiffness and damping properties of each unit. Figure 3 illustrates the deflections of different spring-damper units in the FW suspension under a static external force (a combination of vertical and longitudinal forces or loads). The coordinate of point *B* with respect to the origin *O* is (L, α), where L ($L \geq 0$) is the magnitude of *OB*, and α is the angle of *OB* with respect to the Horizontal Axis *X*; the positive direction of α is assumed to be anti-clockwise.

Stiffness Property of Spring-Damper Unit #*n*:

The displacement D_n of spring-damper unit #*n* can be derived from Fig. 3, such that:

$$D_n = \sqrt{R^2+L^2+2RL\sin(\alpha+2\pi(n-1)/n)} \tag{4}$$

For a particular angle α, the effective stiffness $k_{\alpha n}$ of the spring-damper unit #*n* with respect to L can be formulated from Eq. (4), such that:

$$k_{\alpha n} = K_n\left|\frac{d(D_{ns}-D_n)}{dL}\right| = \frac{K_n|L+R\sin(\alpha+2\pi(n-1)/n)|}{\sqrt{R^2+L^2+2RL\sin(\alpha+2\pi(n-1)/n)}} \tag{5}$$

where D_{ns} is the static displacement of the spring-damper unit #*n* when $L=0$ and $\alpha=0$. K_n is the stiffness coefficient of unit #*n*.

The effective vertical stiffness k_{Vn} of the spring-damper unit #*n* can be derived from Eq. (5) by letting $\alpha=\pi/2$ (or $\alpha=3\pi/2$) and $L=y$, such that:

$$k_{Vn} = \begin{cases} \dfrac{K_n|y + R\cos(2\pi(n-1)/n)|}{\sqrt{R^2 + y^2 + 2Ry\cos(2\pi(n-1)/n)}} & (\alpha = \pi/2) \\ \dfrac{K_n|y - R\cos(2\pi(n-1)/n)|}{\sqrt{R^2 + y^2 - 2Ry\cos(2\pi(n-1)/n)}} & (\alpha = 3\pi/2) \end{cases} \tag{6}$$

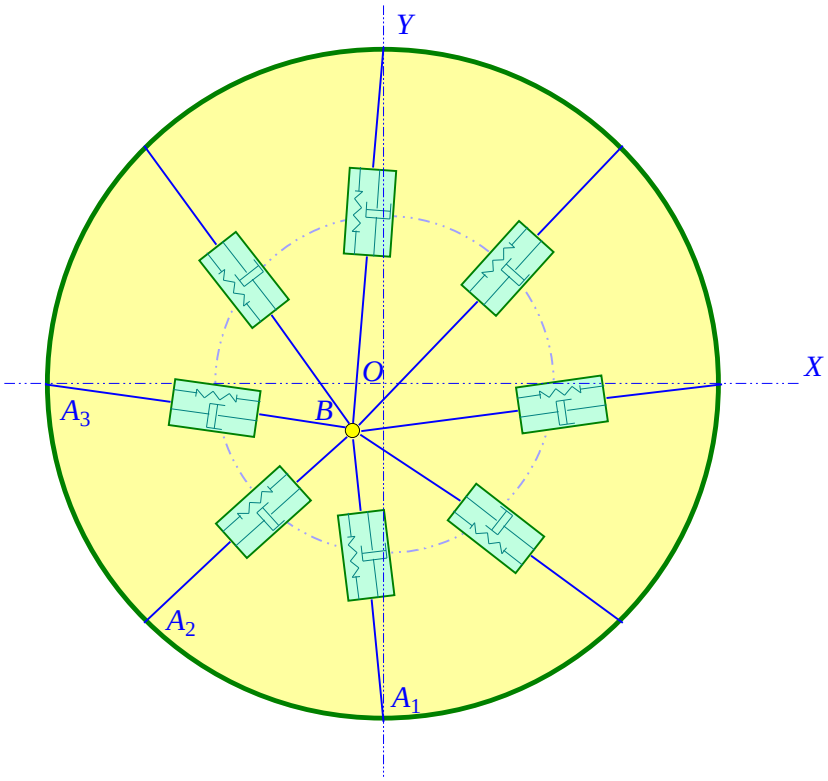

Fig. 3: Representation of deflections of the FW suspension units under a static external force (without considering wheel-hub dimensions).

The effective longitudinal stiffness k_{Xn} of the spring-damper unit #*n* can also be easily derived from Eq. (5) by letting $\alpha = 0$ (or $\alpha = \pi$) and $L = x$, such that:

$$k_{Xn} = \begin{cases} \dfrac{K_n|x + R\sin(2\pi(n-1)/n)|}{\sqrt{R^2 + x^2 + 2Rx\sin(2\pi(n-1)/n)}} & (\alpha = 0) \\ \dfrac{K_n|x - R\sin(2\pi(n-1)/n)|}{\sqrt{R^2 + x^2 - 2Rx\sin(2\pi(n-1)/n)}} & (\alpha = \pi) \end{cases} \tag{7}$$

For a particular magnitude L, the effective rotational stiffness k_{Ln} of the spring-damper unit #*n* with respect to α can be formulated from Equation (16), such that:

$$k_{Ln} = K_n L^2 \left|\frac{d(D_{ns} - D_n)}{d\alpha}\right| = \frac{K_n R L^3 |\cos(\alpha + 2\pi(n-1)/n)|}{\sqrt{R^2 + L^2 + 2RL\sin(\alpha + 2\pi(n-1)/n)}} \tag{8}$$

Stiffness Property of the FW Suspension:

The overall stiffness properties of the FW suspension can be derived from Eqs. (4) to (8). For a translational direction with a given angle α, the effective stiffness k_α of the FW suspension system can be formulated as:

$$k_\alpha = k_{\alpha 1} + k_{\alpha 2} + \cdots + k_{\alpha n} = \sum_{j=1}^{n} \frac{K_j |L + R\sin(\alpha + 2\pi(j-1)/n)|}{\sqrt{R^2 + L^2 + 2RL\sin(\alpha + 2\pi(j-1)/n)}} \tag{9}$$

Assuming the stiffness values of different spring-damper units are identical (and equal to K), Equation (9) can be simplified as:

$$k_\alpha = K \sum_{j=1}^{n} \frac{|L + R\sin(\alpha + 2\pi(j-1)/n)|}{\sqrt{R^2 + L^2 + 2RL\sin(\alpha + 2\pi(j-1)/n)}} \tag{10}$$

The effective vertical stiffness k_V of the FW suspension can be derived from Eq. (10) by letting $\alpha = \pi/2$ (or $\alpha = 3\pi/2$) and $L = y$, such that:

$$k_V = \begin{cases} K \sum_{j=1}^{n} \frac{|y + R\cos(2\pi(j-1)/n)|}{\sqrt{R^2 + y^2 + 2Ry\cos(2\pi(j-1)/n)}} & (\alpha = \pi/2) \\ K \sum_{j=1}^{n} \frac{|y - R\cos(2\pi(j-1)/n)|}{\sqrt{R^2 + y^2 - 2Ry\cos(2\pi(j-1)/n)}} & (\alpha = 3\pi/2) \end{cases} \tag{11}$$

The effective longitudinal stiffness k_X of the FW suspension can also be easily derived from Eq. (10) by letting $\alpha = 0$ (or $\alpha = \pi$) and $L = x$, such that:

$$k_X = \begin{cases} K \sum_{j=1}^{n} \frac{|x + R\sin(2\pi(j-1)/n)|}{\sqrt{R^2 + x^2 + 2Rx\sin(2\pi(j-1)/n)}} & (\alpha = 0) \\ K \sum_{j=1}^{n} \frac{|x - R\sin(2\pi(j-1)/n)|}{\sqrt{R^2 + x^2 - 2Rx\sin(2\pi(j-1)/n)}} & (\alpha = \pi) \end{cases} \tag{12}$$

For a rotational direction with a given magnitude L, the effective rotational stiffness k_L of the FW suspension can be formulated as:

$$k_L = k_{L1} + k_{L2} + \cdots + k_{Ln} = \sum_{j=1}^{n} \frac{K_j R L^3 |\cos(\alpha + 2\pi(j-1)/n)|}{\sqrt{R^2 + L^2 + 2RL\sin(\alpha + 2\pi(j-1)/n)}} \tag{13}$$

Assuming the stiffness values of different spring-damper units are identical (and equal to *K*), Equation (13) can be simplified as:

$$k_L = KRL^3 \sum_{j=1}^{n} \frac{|\cos(\alpha + 2\pi(j-1)/n)|}{\sqrt{R^2 + L^2 + 2RL\sin(\alpha + 2\pi(j-1)/n)}} \tag{14}$$

Damping Property of Spring-Damper Unit #*n*:

For a translational direction with a particular angle α, the effective damping coefficient $C_{\alpha n}$ of the spring-damper unit #*n* can be formulated from Eq. (4), such that:

$$V_n = \frac{dD_n}{dt} = \frac{L\dot{L} + R\dot{L}\sin(\alpha + 2\pi(n-1)/n)}{\sqrt{R^2 + L^2 + 2RL\sin(\alpha + 2\pi(n-1)/n)}}$$

$$C_{\alpha n} = C_n \left|\frac{dV_n}{d\dot{L}}\right| = \frac{C_n|L + R\sin(\alpha + 2\pi(n-1)/n)|}{\sqrt{R^2 + L^2 + 2RL\sin(\alpha + 2\pi(n-1)/n)}} \tag{15}$$

For a rotational direction with a particular magnitude *L*, the effective rotational damping c_{L1} of the spring-damper unit #1 can be formulated from Eq. (4), such that:

$$V_n = \frac{dD_n}{dt} = \frac{RL\dot{\alpha}\cos(\alpha + 2\pi(n-1)/n)}{\sqrt{R^2 + L^2 + 2RL\sin(\alpha + 2\pi(n-1)/n)}}$$

$$c_{Ln} = C_n L^2 \left|\frac{dV_n}{d\dot{\alpha}}\right| = \frac{C_n RL^3|\cos(\alpha + 2\pi(n-1)/n)|}{\sqrt{R^2 + L^2 + 2RL\sin(\alpha + 2\pi(n-1)/n)}} \tag{16}$$

Comparisons between Eqs. (5) and (8) and Eqs. (15) and (16) show that the formulations for the stiffness and damping properties exhibit a similarity. Therefore, the damping property of the FW suspension concept can be derived in a similar manner to those presented in Eqs. (9) to (14), which are summarized below.

Damping Property of the FW Suspension:

For a translational direction with a given angle α, the effective damping c_α of the FW suspension can be derived as:

$$c_\alpha = c_{\alpha 1} + c_{\alpha 2} + \cdots + c_{\alpha n} = \sum_{j=1}^{n} \frac{C_j|L + R\sin(\alpha + 2\pi(j-1)/n)|}{\sqrt{R^2 + L^2 + 2RL\sin(\alpha + 2\pi(j-1)/n)}} \tag{17}$$

Assuming the damping coefficients of different spring-damper units are identical (and equal to *C*), Equation (17) can be simplified as:

$$c_\alpha = C\sum_{j=1}^{n}\frac{|L + R\sin(\alpha + 2\pi(j-1)/n)|}{\sqrt{R^2 + L^2 + 2RL\sin(\alpha + 2\pi(j-1)/n)}} \tag{18}$$

The effective vertical damping c_V of the FW suspension can be derived from Eq. (18), such that:

$$c_V = \begin{cases} C\sum_{j=1}^{n}\frac{|y + R\cos(2\pi(j-1)/n)|}{\sqrt{R^2 + y^2 + 2Ry\cos(2\pi(j-1)/n)}} & (\alpha = \pi/2) \\ C\sum_{j=1}^{n}\frac{|y - R\cos(2\pi(j-1)/n)|}{\sqrt{R^2 + y^2 - 2Ry\cos(2\pi(j-1)/n)}} & (\alpha = 3\pi/2) \end{cases} \tag{19}$$

The effective longitudinal damping c_X of the FW suspension can also be easily derived, such that:

$$c_X = \begin{cases} C\sum_{j=1}^{n}\frac{|x + R\sin(2\pi(j-1)/n)|}{\sqrt{R^2 + x^2 + 2Rx\sin(2\pi(j-1)/n)}} & (\alpha = 0) \\ C\sum_{j=1}^{n}\frac{|x - R\sin(2\pi(j-1)/n)|}{\sqrt{R^2 + x^2 - 2Rx\sin(2\pi(j-1)/n)}} & (\alpha = \pi) \end{cases} \tag{20}$$

For a rotational direction with a particular magnitude *L*, the effective rotational damping c_L of the FW suspension can be formulated, such that:

$$c_L = c_{L1} + c_{L2} + \cdots + c_{Ln} = \sum_{j=1}^{n}\frac{C_j RL^3|\cos(\alpha + 2\pi(j-1)/n)|}{\sqrt{R^2 + L^2 + 2RL\sin(\alpha + 2\pi(j-1)/n)}} \tag{21}$$

Assuming damping coefficients of different spring-damper units are identical (and equal to *C*), Equation (21) can be simplified as:

$$c_L = CRL^3\sum_{j=1}^{n}\frac{|\cos(\alpha + 2\pi(j-1)/n)|}{\sqrt{R^2 + L^2 + 2RL\sin(\alpha + 2\pi(j-1)/n)}} \tag{22}$$

The generalized formulations of properties of the FW suspension, including the stiffness (Eqs. (9) to (14)) and damping (Eqs. (17) to (22)), allow the fundamental property analyses of different FW suspension designs in a very convenient manner.

2.3 PROPERTY ANALYSES

To facilitate the property analyses of various FW suspension designs, two dimensionless property measures, translational property factor (TPF) and rotational property factor (RPF), are defined as:

$$\text{TPF} = \frac{k_\alpha}{nK} = \frac{c_\alpha}{nC}; \quad \text{RPF} = \frac{k_L}{nKL^2} = \frac{c_L}{nCL^2} \tag{23}$$

These two measures indicate the effective stiffness or damping augment/reduction ratio of an FW suspension configuration involving *n* spring-damper units which are evenly distributed and perpendicular to the wheel rim of the FW suspension. It can be observed from Eqs. (9)~(14) and Eqs. (17)~(22) that selection of FW design parameters (*n*, *K*, *C*, *R*) strongly affects these two property measures (TPF and RPF), and thus fundamental properties of the FW suspension.

For a relative comparison of the effects of the design parameters on the properties of FW suspension concept, a 6-wheeled PSV with a static vertical load of 1200 kg is used by assuming loads are evenly distributed on the six wheels, and *R* is selected to be 0.2 m. By assuming operating on Earth, for different FW suspension designs, the static vertical-mode natural frequency ($f = \frac{1}{2\pi}\sqrt{k_{V0}/m}$) of the sprung mass is selected to be 3 Hz, while the vertical-mode damping ratio $\xi = \frac{c_{V0}}{2\sqrt{mk_{V0}}}$ is selected to be 0.2. The number of spring-damper units involved in an FW suspension is selected to be 3 and 6.

FW Suspension (*n*=3)

For the FW suspension design configuration involving three spring-damper units, the TPF at the origin (*L*=0) can be derived from Eq. (10), such that:

$$\text{TPF}_0 = \frac{1}{3}\sum_{j=1}^{3}|\cos(2\pi(j-1)/3)| = \frac{2}{3} \tag{24}$$

Therefore, the effective vertical stiffness and damping can be obtained from Eq. (24):

$$k_{V0} = 2K; \quad c_{V0} = 2C \tag{25}$$

Corresponding to the static vertical load (200 kg) and vertical-mode natural frequency (3 Hz), the parameters *K* and *C* can be selected as:

$$K = 35{,}495 \text{ N/m}; \; C = 754 \text{ Ns/m} \tag{26}$$

Based on the generalized models, the TPF and RPF can be represented as a function of two parameters: *L* and α, respectively, which are illustrated in Figs. 4 and 5. Since the three spring-damper units are evenly distributed, the property would vary periodically every $2\pi/3$ with respect to α. Therefore, the two property measures presented in Figs. 4 and 5 are only simulated for $\pi/6 \leq \alpha \leq 5\pi/6$. For a given α, the TPF and RPF increase or decrease almost linearly with increasing *L*. However, the TPF and RPF vary considerably for different angles, leading to considerable stiffness variations during driving, which are undesirable for vehicle motion control and dynamic performance and stability. This is due to only three spring-damper units employed in the FW suspension. The results also suggest that for the FW suspension design configuration involving three spring-damper units, an increase in *L* induces a larger

peak-to-peak variation in TPF during a rotational driving cycle, and a higher RPF and thus higher rotational stiffness.

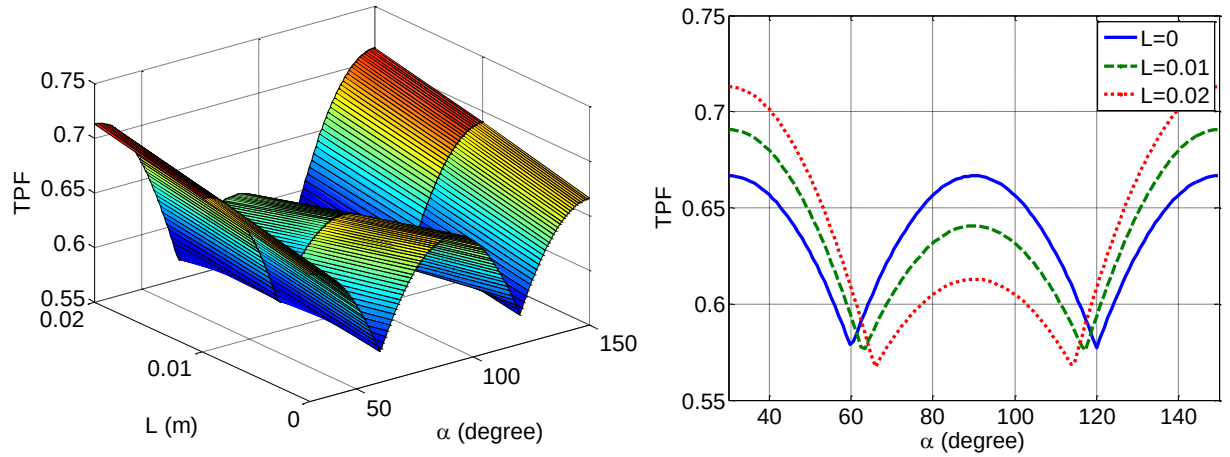

(a) (b)

Fig. 4: TPF of the FW suspension (n=3) as a function of L and α: (a) view I; and (b) view II.

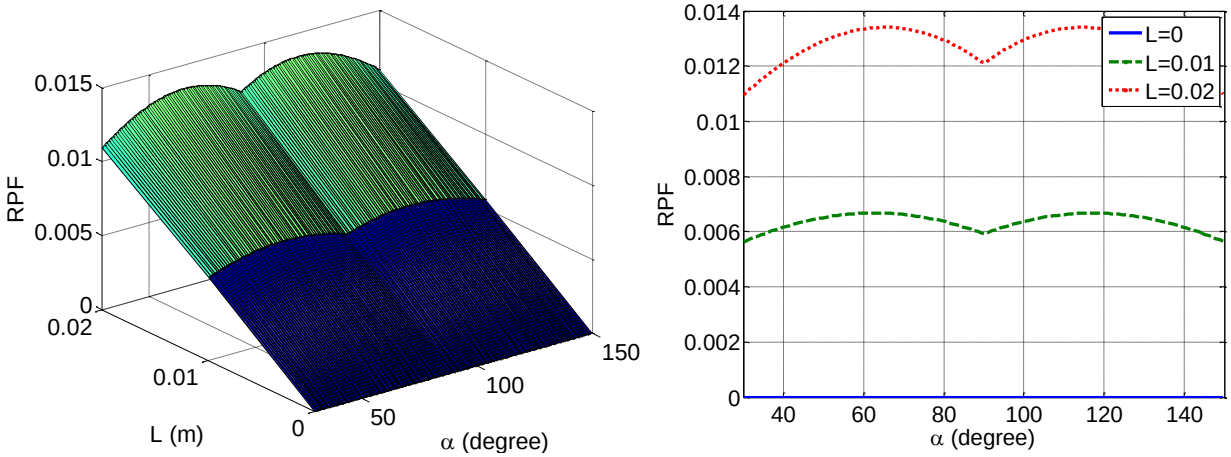

(a) (b)

Fig. 5: RPF of the FW suspension (n=3) as a function of L and α: (a) view I; and (b) view II.

FW Suspension (n=6)

For the FW suspension configuration with six spring-damper units, the TPF at the origin (L=0) can be derived from Eq. (10), such that:

$$\mathrm{TPF}_0 = \frac{2}{3} \tag{27}$$

Therefore, the effective vertical stiffness and damping can be obtained from Eq. (27), such that:

$$k_{V0} = 4K;\ c_{V0} = 4C \tag{28}$$

Considering the static vertical load (200 kg) and vertical-mode natural frequency (3 Hz), the parameters K and C can be designed as:

$$K = 17{,}747\ \text{N/m};\ C = 377\ \text{Ns/m} \tag{29}$$

Figures 6 and 7 presents the TPF and RPF can be obtained as a function of two parameters: L and α, respectively, only for $\pi/6 \leq \alpha \leq \pi/2$. This is due to the fact that since the six spring-damper units are evenly distributed, the property varies periodically every $\pi/3$ with respect to α. Similar to those of the FW suspension design configuration involving three spring-damper units, for a given α, the TPF and RPF increase or decrease nearly linearly with increasing L. The TPF and RPF vary considerably for different angles. However, the results indicate that for the FW suspension design configuration involving six spring-damper units, an increase in L tends to reduce the peak-to-peak variation in TPF during a rotational driving cycle, and a higher RPF.

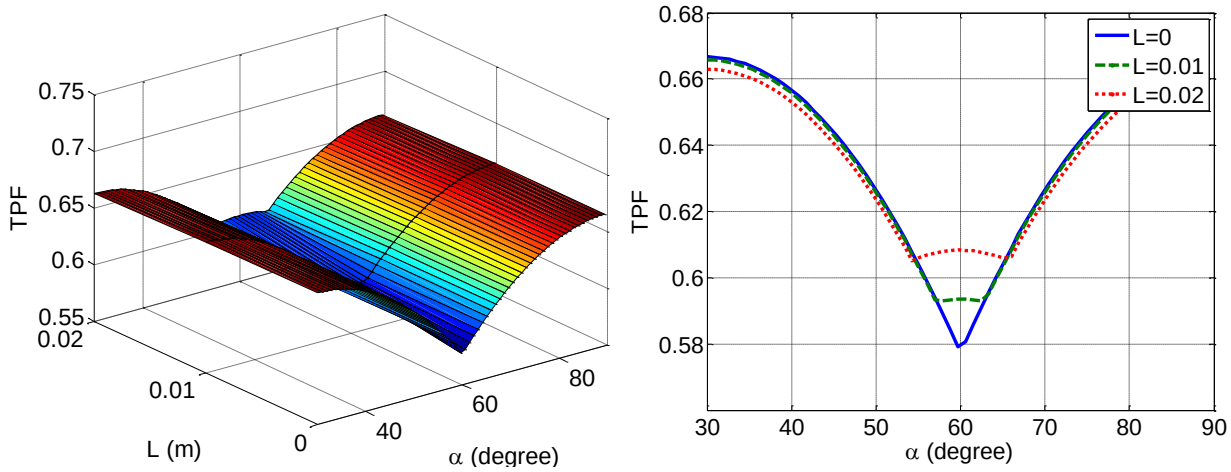

(a) (b)

Fig. 6: TPF of the FW suspension (n=6) as a function of L and α: (a) view I; and (b) view II.

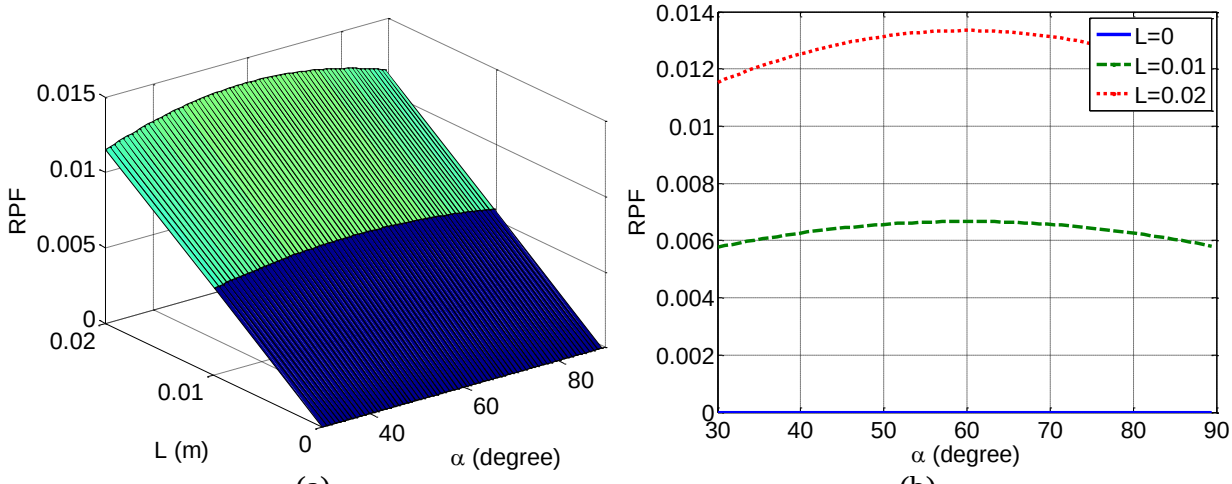

(a) (b)

Fig. 7: RPF of the FW suspension (n=6) as a function of L and α: (a) view I; and (b) view II.

It can be observed from Figs. 4-7 that increasing the number of spring-damper units tends to reduce the variations in the stiffness and damping properties of the FW suspension design configurations. However, an increase in the number of spring-damper units also tends to make the suspension system

heavier and more complex, posing additional difficulties on FW suspension design, in terms of design space and effective suspension travel.

2.4 MODELING OF THE CRR CHARACTERISTICS

Based on the selected design parameters, the power consumption characteristics of different FW suspension design configurations can be conveniently analyzed using Eq. (3). In order to simply the analysis, the compliance rolling resistance (CRR) coefficient for an FW suspension is defined and derived from Eq. (3), assuming an adequately long time-period ($\omega T = 2i\pi$), such that:

$$\mathrm{CRR}_{FW} = \frac{F_{AVE}}{Mg} = \frac{P_{S_{AVE}}/V}{Mg} = \frac{R^2 L_0^2}{2\pi g}\frac{V}{(R-L_0)^2}\frac{nC}{M}\frac{\int_0^{2i\pi}\frac{\sin^2(q)}{R^2+L_0^2-2RL_0\cos(q)}d(q)}{i}$$
$$= \frac{\left(\frac{R}{L_0}\right)^2}{2\pi g}\frac{V}{\left(\frac{R}{L_0}-1\right)^2}\frac{nC}{M}\frac{\int_0^{2i\pi}\frac{\sin^2(q)}{\left(\frac{R}{L_0}\right)^2+1-2\left(\frac{R}{L_0}\right)\cos(q)}d(q)}{i} \tag{30}$$

From Eq. (23), it can be obtained that:

$$\mathrm{TPF}_0 = \frac{c_{V0}}{nC} \tag{31}$$

Therefore, the following relation can be formulated based on Eq. (31), such that:

$$\frac{nC}{M} = \frac{c_{V0}}{M\mathrm{TPF}_0} = \frac{4\pi\xi f}{\mathrm{TPF}_0} \tag{32}$$

By assuming small static deflection of FW suspension, it can also be obtained that:

$$L_0 = \frac{Mg}{k_{V0}} = \frac{g}{4\pi^2 f^2} \tag{33}$$

By assuming $d = R/L_0$, the mathematical formulation of CRR_{FW} can be obtained based on Eqs. (30), (32) and (33), such that:

$$\mathrm{CRR}_{FW} = \frac{2\pi\xi f V}{g(d-1)^2\mathrm{TPF}_0} \tag{34a}$$

Or

$$\mathrm{CRR}_{FW} = \frac{g}{8\pi^3}\frac{\xi f V}{\left(Rf^2 - \frac{g}{4\pi^2}\right)^2 \mathrm{TPF}_0} \tag{34b}$$

Equation (34a) suggests that the CRR_{FW} of an FW suspension is a function of gravity, static vertical natural frequency and damping ratio, vehicle driving speed, TPF_0, and the ratio of the FW suspension wheel radius (R) to the static deflection (L_0). Equation (34b) suggests that the CRR_{FW} of an FW suspension is a function of gravity, static vertical natural frequency and damping ratio, driving speed, TPF_0, and the FW suspension wheel radius (R).

3. Modeling Generalization of FW Suspension Considering Wheel-Hub Dimensions

The above section has developed generalized models of suspension properties, power consumption characteristics and CRR for the FW suspension concept by assuming the negligible wheel-hub dimensions. However, the practical design of an FW suspension usually employs a wheel-hub, which would be expected to induce additional effect on suspension properties, power consumption characteristics and CRR of the FW suspension. This section extends the generalized models of suspension properties, power consumption characteristics and CRR to the FW suspension considering wheel-hub dimensions. Figure 8 presents the design of the FW suspension concept, where a number of spring-damper units are assumed to be ideally perpendicular to the wheel rim and evenly distributed when the external loads are not applied. The other ends of the units are assumed to be connected to the circular wheel-hub (radius r). The deflections of different spring-damper units of the FW suspension subject to a static vertical load and a constant driving speed are shown in Fig. 8.

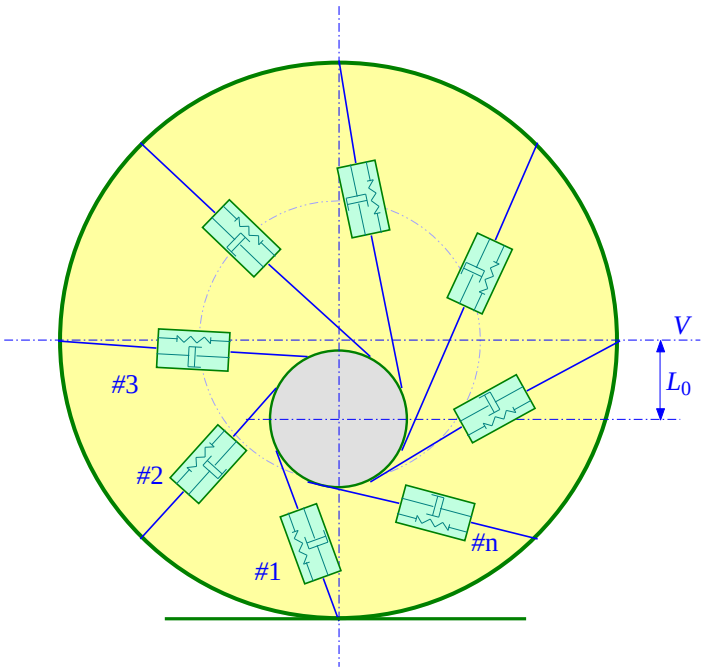

Fig. 8: Representation of the FW suspension deflections subject to a static vertical load and a constant forward speed (considering wheel-hub dimensions).

3.1 MODELING OF POWER CONSUMPTION CHARACTERISTICS

Figure 9 presents an equivalent model of motion of a single spring-damper unit in an FW suspension, to derive the generalized models of the FW suspension. By assuming n spring-damper units involved in an FW suspension, the motions of different spring-damper units can be derived based on Figs. 8 and 9.

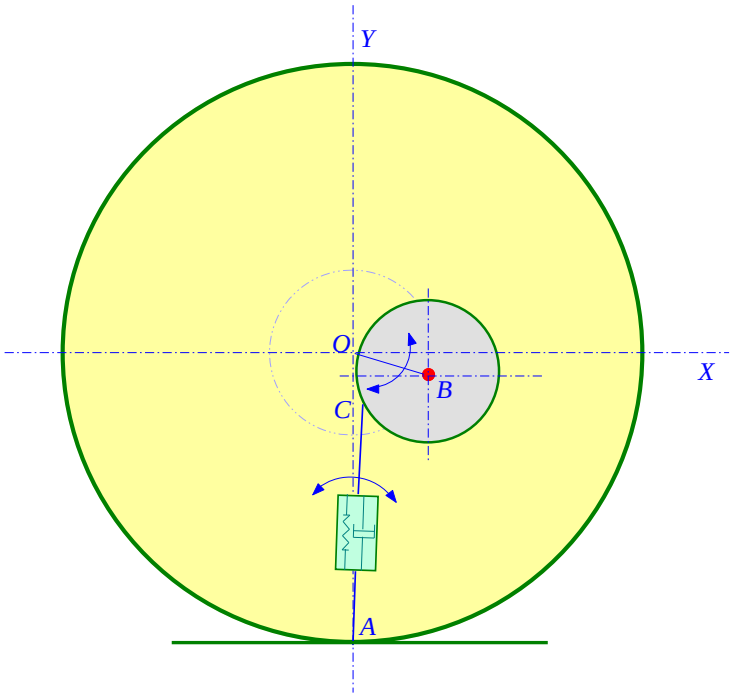

Fig. 9: Modeling simplification of the FW suspension (considering wheel-hub dimensions).

The displacement and velocity, and thus power consumption of the spring-damper unit #n in an FW suspension can be formulated by considering a constant vehicle forward speed and a static vertical load, such that:

$$D_n = \sqrt{R_{eq}^2 + L_0^2 - 2R_{eq}L_0\cos(\omega t + \gamma_0 + 2\pi(j-1)/n)}$$

$$V_n = \frac{dD_n}{dt} = \frac{R_{eq}L_0\omega\sin(\omega t + \gamma_0 + 2\pi(j-1)/n)}{\sqrt{R_{eq}^2 + L_0^2 - 2R_{eq}L_0\cos(\omega t + \gamma_0 + 2\pi(j-1)/n)}}$$

$$P_n = C_n V_n^2 = C_n \frac{R_{eq}L_0^2\omega^2 sin^2(\omega t + \gamma_0 + 2\pi(j-1)/n)}{R_{eq}^2 + L_0^2 - 2R_{eq}L_0\cos(\omega t + \gamma_0 + 2\pi(j-1)/n)} \tag{35}$$

where β_0 is the angle between BC and the Horizontal Axis X when the system is static and there is no external force applied. R_{eq} and γ_0 are given below:

$$R_{eq} = \sqrt{R^2 + r^2 + 2Rr\sin\beta_0}; \quad \gamma_0 = \arctan(r\cos\beta_0/(R + r\sin\beta_0)) \tag{36}$$

By comparing the above equation with Eq. (1), it can be seen that the only differences between the two equations are R and R_{eq}, and a phase lead γ_0. Assuming $r = 0$, then $R_{eq} = R$, and $\gamma_0 = 0$, based on which Eq. (36) is identical to Eq. (1). Therefore, the power consumption of the FW suspension

considering wheel hub can be derived in a very similar manner to those presented in Section 2, which is summarized below.

Power Consumption of FW Suspension:
The overall power consumption of the FW suspension considering wheel-hub dimensions can be derived, such that:

$$P_S = \sum_{j=1}^{n} \frac{C_j R_{eq}^2 L_0^2 \omega^2 \sin^2(\omega t + \gamma_0 + 2\pi(j-1)/n)}{R_{eq}^2 + L_0^2 - 2R_{eq}L_0 \cos(\omega t + \gamma_0 + 2\pi(j-1)/n)} \tag{37}$$

Assuming damping coefficients of different spring-damper units are equal to *C*, the average power consumption can be derived from Eq. (37) for an adequately long time-period, such that:

$$P_{S_{AVE}} = \frac{nCR^2L_0^2\omega}{T} \int_0^{\omega T} \frac{\sin^2(q)}{R_{eq}^2 + L_0^2 - 2R_{eq}L_0 \cos(q)} d(q) \tag{38}$$

The above formulation indicates that the power consumption of the FWS system is directly related to the number of spring-damper units, the damping coefficient of each unit, the radius of the FW suspension wheel, the radius of the FWS wheel hub, the angular position of the spring-damper unit connected to the wheel hub, the static vertical deflection as well as the driving speed.

3.2 MODELING OF STIFFNESS AND DAMPING PROPERTIES
Figure 10 illustrates the deflections of different spring-damper units in an FW suspension under a static external force. The coordinate of point *B* with respect to the origin *O* is (L, α), where *L* is the magnitude of *OB*, and α is the angle of *OB* with respect to the Horizontal Axis *X*; the positive direction of α is assumed to be anti-clockwise.

Stiffness Property of Spring-Damper Unit #*n*:
The displacement of the spring-damper unit #*n* can be derived from Fig. 10, such that:

$$D_n = \sqrt{R_{eq}^2 + L^2 - 2R_{eq}L\sin(\alpha + \gamma_0 + 2\pi(n-1)/n)} \tag{39}$$

where R_{eq} and γ_0 are given in Eq. (54). By comparing the above equation with Eq. (6), it can be seen that the only differences between the two equations are *R* and R_{eq}, and a phase lead γ_0. Assuming $r = 0$, then $R_{eq} = R$, and $\gamma_0 = 0$, based on which Eq. (57) can be simplified and identical to Eq. (6). Therefore, the suspension properties of the FW suspension considering wheel-hub dimensions can be derived in a very similar manner to those presented in Section 2, which are briefly summarized below.

Stiffness Property of the FW Suspension:
For a translational direction with a given angle α, the effective stiffness of the FW suspension can be derived, such that:

$$k_\alpha = k_{\alpha 1} + k_{\alpha 2} + \cdots + k_{\alpha n} = \sum_{j=1}^{n} \frac{K_j \left| L + R_{eq} \sin(\alpha + \gamma_0 + 2\pi(j-1)/n) \right|}{\sqrt{R_{eq}^2 + L^2 + 2R_{eq} L \sin(\alpha + \gamma_0 + 2\pi(j-1)/n)}} \tag{40}$$

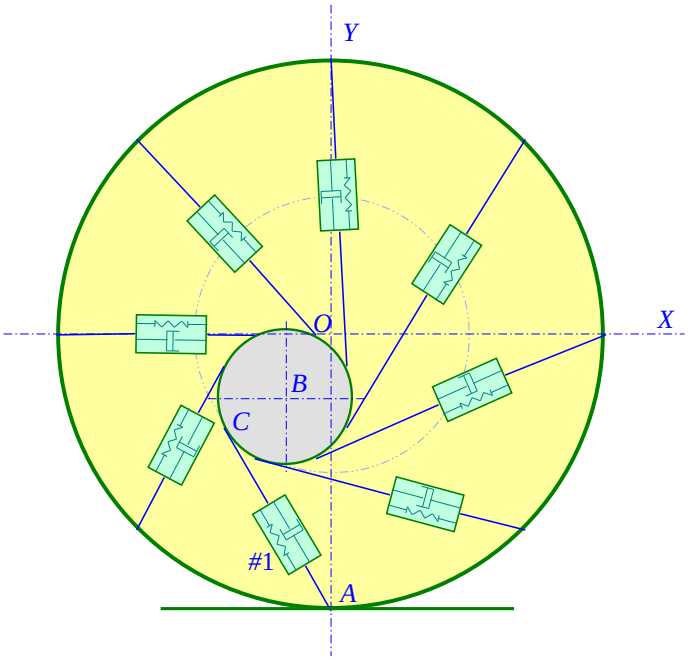

Fig. 10: Representation of deflections of the FW suspension units under a static external force (considering wheel-hub dimensions).

Assuming stiffness values of different spring-damper units are equal to *K*, Equation (40) can be further simplified as:

$$k_\alpha = K \sum_{j=1}^{n} \frac{\left| L + R_{eq} \sin(\alpha + \gamma_0 + 2\pi(j-1)/n) \right|}{\sqrt{R_{eq}^2 + L^2 + 2R_{eq} L \sin(\alpha + \gamma_0 + 2\pi(j-1)/n)}} \tag{41}$$

The effective vertical stiffness of the FW suspension can be derived from Eq. (41) simply by letting $\alpha = \pi/2$ (or $\alpha = 3\pi/2$) and $L = y$. The effective longitudinal stiffness of the FW suspension also be easily derived from Eq. (41) by letting $\alpha = 0$ (or $\alpha = \pi$) and $L = x$.

For a rotational direction with a given magnitude *L*, the effective rotational stiffness of the FW suspension can be formulated, such that:

$$k_L = k_{L1} + k_{L2} + \cdots + k_{Ln} = \sum_{j=1}^{n} \frac{K_j R_{eq} L^3 \left| \cos(\alpha + \gamma_0 + 2\pi(j-1)/n) \right|}{\sqrt{R_{eq}^2 + L^2 + 2R_{eq} L \sin(\alpha + \gamma_0 + 2\pi(j-1)/n)}} \tag{42}$$

Assuming stiffness values of different spring-damper units are identical (and equal to *K*), Equation (42) can be simplified as:

$$k_L = KR_{eq}L^3 \sum_{j=1}^{n} \frac{|\cos(\alpha + \gamma_0 + 2\pi(j-1)/n)|}{\sqrt{R_{eq}^2 + L^2 + 2R_{eq}L\sin(\alpha + \gamma_0 + 2\pi(j-1)/n)}} \tag{43}$$

Damping Property of the FW Suspension:

For a translational direction with a particular angle α, the effective damping of the FW suspension can be derived as:

$$c_\alpha = c_{\alpha 1} + c_{\alpha 2} + \cdots + c_{\alpha n} = \sum_{j=1}^{n} \frac{C_j\left|L + R_{eq}\sin(\alpha + \gamma_0 + 2\pi(j-1)/n)\right|}{\sqrt{R_{eq}^2 + L^2 + 2R_{eq}L\sin(\alpha + \gamma_0 + 2\pi(j-1)/n)}} \tag{44}$$

Assuming the damping coefficients of different spring-damper units are equal to C, Equation (64) can be simplified as:

$$c_\alpha = C \sum_{j=1}^{n} \frac{\left|L + R_{eq}\sin(\alpha + \gamma_0 + 2\pi(j-1)/n)\right|}{\sqrt{R_{eq}^2 + L^2 + 2R_{eq}L\sin(\alpha + \gamma_0 + 2\pi(j-1)/n)}} \tag{45}$$

For a rotational direction with a particular magnitude L, the effective rotational damping of the FW suspension can be formulated, such that:

$$c_L = c_{L1} + c_{L2} + \cdots + c_{Ln} = \sum_{j=1}^{n} \frac{C_j R_{eq}L^3|\cos(\alpha + \gamma_0 + 2\pi(j-1)/n)|}{\sqrt{R_{eq}^2 + L^2 + 2R_{eq}L\sin(\alpha + \gamma_0 + 2\pi(j-1)/n)}} \tag{46}$$

Assuming damping coefficients of different spring-damper units are equal to C, Equation (46) can be simplified as:

$$c_L = CR_{eq}L^3 \sum_{j=1}^{n} \frac{|\cos(\alpha + \gamma_0 + 2\pi(j-1)/n)|}{\sqrt{R_{eq}^2 + L^2 + 2R_{eq}L\sin(\alpha + \gamma_0 + 2\pi(j-1)/n)}} \tag{47}$$

The generalized formulations of FW suspension properties considering wheel-hub dimensions allow the property analyses of alternative FW suspension designs in a very convenient manner. It should also be noted that introducing wheel-hub radius and the angular positions of the spring-damper units connected to the wheel hub provides two more design parameters for tuning suspension properties and thus improve the design flexibility of the FW suspension.

3.3 MODELING OF THE CRR CHARACTERISTICS

The CRR coefficient for an FW suspension considering wheel hub can be derived from Eq. (38), assuming an adequately long time-period ($\omega T = 2i\pi$), such that:

$$\mathrm{CRR}_{FW} = \frac{R_{eq}^2 L_0^2}{2\pi g} \frac{V}{\left(R_{eq} - L_0\right)^2} \frac{nC}{M} \frac{\int_0^{2i\pi} \frac{\sin^2(q)}{R_{eq}^2 + L_0^2 - 2R_{eq}L_0\cos(q)} d(q)}{i}$$

$$= \frac{\left(\frac{R_{eq}}{L_0}\right)^2}{2\pi g} \frac{V}{\left(\frac{R_{eq}}{L_0} - 1\right)^2} \frac{nC}{M} \frac{\int_0^{2i\pi} \frac{\sin^2(q)}{\left(\frac{R_{eq}}{L_0}\right)^2 + 1 - 2\left(\frac{R_{eq}}{L_0}\right)\cos(q)} d(q)}{i} \tag{48}$$

By assuming $d = R_{eq}/L_0$, the mathematical formulation of CRR_{FW} can be obtained based on Eqs. (32), (33) and (48), such that:

$$\mathrm{CRR}_{FW} = \frac{2\pi\xi f V}{g(d-1)^2 \mathrm{TPF}_0} \tag{49a}$$

Or

$$\mathrm{CRR}_{FW} = \frac{g}{8\pi^3} \frac{\xi f V}{\left(R_{eq} f^2 - \frac{g}{4\pi^2}\right)^2 \mathrm{TPF}_0} \tag{49b}$$

By comparing Eqs. (34) and (49), it can be clearly seen that the only difference between the two equations is R and R_{eq}.

3.4 SENSITIVITY ANALYSES OF THE CRR CHARACTERISTICS

Equation (49b) indicates that there are a number of parameters affecting the compliance rolling resistance of FW suspension and thus its power consumption characteristics. It would be beneficial to investigate the effects of these parameters on the CRR of FW suspension. It can be seen that the CRR_{FW} is proportional to the effective vertical damping ratio (ξ) and rover forward speed (V), and $1/\mathrm{TPF}_0$.

The following formulation can be obtained from Eq. (49b), such that:

$$\frac{\partial \mathrm{CRR}_{FW}}{\partial g} = \frac{\xi f V}{8\pi^3 \mathrm{TPF}_0} \frac{R_{eq} f^2 + \frac{g}{4\pi^2}}{\left(R_{eq} f^2 - \frac{g}{4\pi^2}\right)^3} \tag{50}$$

The static deflection L_0 is generally far less than R_{eq} for practical designs of conventional wheel and FW suspension, so it can be derived from Eq. (48) that $d > 1$. By comparing Eqs. (49a) and (49b), it can be obtained that $R_{eq} f^2 - \frac{g}{4\pi^2} > 0$. Therefore, it can be derived from Eq. (50) that:

$$\frac{\partial \mathrm{CRR}_{FW}}{\partial g} = \frac{\xi f V}{8\pi^3 \mathrm{TPF}_0} \frac{R_{eq} f^2 + \frac{g}{4\pi^2}}{\left(R_{eq} f^2 - \frac{g}{4\pi^2}\right)^3} > 0 \tag{51}$$

The above formulation indicates that a higher gravity increases the CRR of the FW suspension, while the gravity characteristics depend upon the planet surface explored.

It can also be obtained from Eq. (49b) that:

$$\frac{\partial \mathrm{CRR}_{FW}}{\partial f} = -\frac{g \xi V}{8\pi^3 \mathrm{TPF}_0} \frac{\frac{g}{4\pi^2} + 3R_{eq} f^2}{\left(R_{eq} f^2 - \frac{g}{4\pi^2}\right)^3} \tag{52}$$

Since $R_{eq} f^2 - \frac{g}{4\pi^2} > 0$, it can be derived from Eq. (52) that:

$$\frac{\partial \mathrm{CRR}_{FW}}{\partial f} = -\frac{g \xi V}{8\pi^3 \mathrm{TPF}_0} \frac{\frac{g}{4\pi^2} + 3R_{eq} f^2}{\left(R_{eq} f^2 - \frac{g}{4\pi^2}\right)^3} < 0 \tag{53}$$

The above formulation indicates that a higher vertical-mode natural frequency help decrease the CRR of the FW suspension. However, a higher vertical-mode natural frequency means a stiffer FW suspension, and thus generally reduced vibrations- and shock-isolation performance.

Eq. (72b) yields:

$$\frac{\partial \mathrm{CRR}_{FW}}{\partial R_{eq}} = -\frac{g \xi f V}{8\pi^3 \mathrm{TPF}_0} \frac{f^2}{\left(R_{eq} f^2 - \frac{g}{4\pi^2}\right)^3} \tag{54}$$

Since $R_{eq} f^2 - \frac{g}{4\pi^2} > 0$, it can be derived from Eq. (54) that:

$$\frac{\partial \mathrm{CRR}_{FW}}{\partial R_{eq}} = -\frac{g \xi f V}{8\pi^3 \mathrm{TPF}_0} \frac{f^2}{\left(R_{eq} f^2 - \frac{g}{4\pi^2}\right)^3} < 0 \tag{55}$$

The above formulation indicates that a larger R_{eq} decreases the CRR of the FW suspension. While the FW suspension wheel radius R is limited by the PSV design and system packaging, a proper selection of wheel-hub radius r and the angle β_0 would help to increase R_{eq}, and thus reduce the CRR and power consumption of the FW suspension. This also partially suggests the design flexibility of FW suspension.

The CRR_{FW} values of an FW suspension can be effectively evaluated based on Eq. (49b). An FW suspension involving six spring-damper units is used for calculating and comparing the CRR_{FW} values, which are summarized in Table 1. The results suggest that selection/design of different wheel hub radius and the angular positions of the spring-damper units connected to the wheel hub could considerably vary the CRR_{FW} values of the FW suspension configurations, which however is constrained by the practical design considerations, such as the FW suspension wheel size and design space for effective suspension travels of each spring-damper unit. The results further demonstrate that the gravity characteristics have a very strong effect on power consumption of FW suspension. When operating on Mars, the power consumption due to the FW suspension would be expected to be much lower than that on Earth.

Table 1: Comparison of CRR_{FW} of a 6-wheeled PSV integrating different FW suspension designs.

M (kg)	f (Hz)	ξ	R (cm)	r (cm)	β_0	g (m/s^2)	V (m/s)	CRR_{FW}	Power consumption (W)
1200	4	0.2	20	6	0	9.81 (Earth)	2	0.01	118
				6	$\pi/2$			0.0062	73
				6	π			0.01	118
				6	$3\pi/2$			0.024	283
				6	0	3.71 (Mars)		0.0034	15
				6	$\pi/2$			0.0022	10
				6	π			0.0034	15
				6	$3\pi/2$			0.0078	35

4. Conclusions

This study developed generalized analytical models for fundamental stiffness/damping properties as well as power consumption characteristics of flexible-wheel suspension concept for planetary surface vehicles. Based on the modeling generalization and two proposed dimensionless property measures, translational property factor (TPF) and rotational property factor (RPF), the properties of two selected flexible-wheel suspension design configurations (involving different numbers of units) were analyzed and compared. The results demonstrated that employing more spring-damper units would yield less variation in suspension stiffness and damping, which however tends to increase the suspension complexity and weight. The compliance rolling resistance coefficient was further defined and derived for the flexible-wheel suspension concept.

The generalized models for the flexible-wheel suspension considering practical wheel-hub dimensions were also derived. The sensitivity analyses were further conducted to investigate the effects of different design and operating parameters on the compliance rolling resistance and power consumption characteristics of different FW suspension designs. The results indicated that the involvement of wheel hub with a particular radius provides two additional design parameters for suspension property tuning. These two design parameters also strongly affect the compliance rolling resistance of the flexible-wheel suspension, where an appropriate selection/design of the two parameters would yield considerably improved power consumption characteristics for the flexible-wheel suspension. The effects of the gravity characteristics due to different planets on the compliance rolling resistance and power consumption of FW suspension designs were also demonstrated, where a lower gravity value yields lower compliance rolling resistance and thus power consumption. The modeling generalization developed in this study permits analyses of fundamental stiffness/damping properties and power consumption characteristics of various flexible-wheel suspension designs in a uniform and very

convenient manner, which would also serve as a theoretical foundation for the design of the flexible-wheel suspension for future planetary surface vehicles.

References:

1. Tompkins, P., 2005, 'Mission-directed path planning for planetary rover exploration', PhD Thesis, Carnegie Mellon University, PA, USA.
2. Heverly, M. and Matthews, J., 2008, 'A wheel-on-limb rover for lunar operation', Proceedings of the 9th International Symposium on Artificial Intellengence, Robotics and Automation in Space, Los Angeles, CA, USA.
3. Michaud, S., Gibbesch, A., Thueer, T., Krebs, A., Lee, C., Despont, B., Schafer, B. and Slade, R., 2008, 'Development of the ExoMars chassis and locomotion subsystem', Proceedings of the 10th ESA Workshop on Advanced Space Technologies for Robotics and Automation, Noordwijk, The Netherlands.
4. Tompkins, P., Stentz, T., and Whittaker, W., 2001, 'Automated surface mission planning considering terrain, shadows, resources and time', Proceedings of the 6th International Symposium on Artificial Intelligence, Robotics and Automation in Space (I-SAIRAS), Montreal, Canada.
5. Harrison, D., Ambrose, R., Bluethmann, B. and Junkin, L., 2007, 'Next generation rover for lunar exploration', IEEE Aerospace Conference, Big Sky, MT, USA.
6. Bauer, R., Leung, W. and Barfoot, T., 2005, 'Development of a dynamic simulation tool for the Exomars rover', Proceeding of the 8th International Symposium on Artificial Intelligence, Robotics and Automation in Space, Munchen, Germany.
7. Kucherenko, V., Bogatchev, A. and Winnendael, M., 2004, 'Chassis concepts for the exomars rover', Proceedings of the 8th ESA Workshop on Advanced Space Technologies for Robotics and Automation, Noordwijk, The Netherlands.
8. Gibbesch, A and Schafer, B., 2004, 'Advanced modeling and simulation methods of planetary rover mobility on soft terrain', Proceedings of the 8th ESA Workshop on Advanced Space Technologies for Robotics and Automation, Noordwijk, The Netherlands.
9. Graham, J.B., 2007, 'Prospecting rovers for lunar exploration', IEEE Aerospace Conference, Big Sky, MT, USA.
10. Michaud, S., Richter, L., Patel, N., Thueer, T., Hulsing, T., Joudrier, L. Siegwart, R. and Ellery, A., 2004, 'RCET: rover chassis evaluation tools', Proceedings of the 8th ESA Workshop on Advanced Space Technologies for Robotics and Automation, Noordwijk, The Netherlands.
11. Patel, N., Ellery, A., Allouis, E., Sweeting, M. and Richter, L., 2004, 'Rover mobility performance evaluation tool (RMPET): a systematic tool for rover chassis evaluation via application of Bekker theory', Proceedings of the 8th ESA Workshop on Advanced Space Technologies for Robotics and Automation, Noordwijk, The Netherlands.
12. Thueer, T. and Siegwart, R., 2007, 'Evaluation and optimization of rover locomotion performance', Workshop on Space Robotics, ICRA'07, Rome, Italy.
13. Ahmadian, M., 1999, 'On the isolation properties of semiactive dampers', Journal of Vibration and Control, 5, p. 217-232.
14. Fu, T.-T. and Cebon, D., 2003, 'Economic evaluation and the design of vehicle suspensions', International Journal of Vehicle Design, 31, p. 125-161.
15. Song, X., Ahmadian, M., Southward, S.C., and Miller, L., 2005, 'An adaptive semiactive control algorithm for magneto-rheological suspension systems', ASME Journal of Vibration and Acoustic, 127(5), p. 493-502.
16. Cao, D., Rakheja, S. and Su, C.-Y., 2008, 'Dynamic analyses of roll plane interconnected hydro-pneumatic suspension systems,' International Journal of Vehicle Design, 47, p. 51-80.
17. Cao, D., Rakheja, S. and Su, C.-Y., 2008, 'Heavy vehicle pitch dynamics and suspension tuning. Part I: Unconnected suspension', Vehicle System Dynamics, 46, p. 931-953.

18. Song, X., Ahmadian, M. and Southward, S.C., 2007, 'Analysis and strategy for super harmonics with semiactive magneto-rheological suspension systems', ASME Journal of Dynamic Systems, Measurement & Control, 129, p. 795-803.
19. Michaud, S., Hoepflinger, M., Thueer, T., Lee, C., Krebs, A., Despont, B., Gibbesch, A. and Richter, L., 2008, 'Lession learned from exomars locomotion system test campaign', Proceedings of the 10th ESA Workshop on Advanced Space Technologies for Robotics and Automation, Noordwijk, The Netherlands.
20. Favaedi, Y. and Pechev, A., 2008, 'Development of tractive performance prediction for flexible wheel', Proceedings of the 10th ESA Workshop on Advanced Space Technologies for Robotics and Automation, Noordwijk, The Netherlands.
21. Naumann, W., Hofmann, P. and Richter, A., 2002, 'Robots to support a human mars mission', The 7th ESA Workshop on Advanced Space Technologies for Robotics and Automation, Noordwijk, The Netherlands.
22. Lindermann, R. and Voorhees, C., 2005, 'Mars exploration rover mobility assembly design, test and performance', Proceedings of the 2005 IEEE International Conference on Systems, Man and Cybernetics, Hawaii, USA.
23. Gettys, T., 2005, 'Passion for an airless future', SAE100 Future Look, The Future of Mobility Technology, 113(13), p. 84-85.
24. Meruani, A., 2006, 'Tweel^{TW} technology tires for wheelchairs and instrumentation for measuring enerday wheeled mobility', Master Thesis, Georgia Institute of Technology, GA, USA.
25. Raemaekers, A.J.M. and Kerkhoven, J.D.G., 2006, 'Design of a torque measurement device for the ExoMars rover', DCT 2006.125, Master Team Project Report, Technische Universiteit Eindhoven, Eindhoven, the Netherlands.
26. Lakes, R.S., 2002, 'High damping composite materials: effect of structural hierarchy', Journal of composite materials, 36, p. 287-297.